

RESPONSE OF A BURIED CONCRETE PIPELINE TO GROUND RUPTURE: A FULL-SCALE EXPERIMENT AND SIMULATION

Srinivasa S. NADUKURU¹, Junhee KIM¹, Sean O'CONNOR¹, Mohammad POUR-GHAZ²,
Radoslaw L. MICHALOWSKI¹, Jerome P. LYNCH¹, Russell A. GREEN³,
Aaron S. BRADSHAW⁴, and W. Jason WEISS²

ABSTRACT

A typical water distribution system includes a network of steel and concrete pipelines. Concrete segmental pipelines are particularly vulnerable to damage by ground rupture. Ground displacements may produce significant bending in the pipelines, in addition to shear and net tension or compression. A full-scale experiment was performed on a buried segmental concrete pipeline subjected to the ground rupture. The pipeline was buried under a layer of sand in a test tank with length of about 13.4 m. A dense array of sensors including potentiometers, strain gauges, load cells, acoustic emission sensors, magnetic sensors, and tape gauges were installed along the length of the pipeline to measure the pipeline response to ground displacements. Permanent displacement was induced by movement of one portion of the test basin. The test was static in nature, and it was to simulate the fault displacement rather than earthquake shaking. Deformation of the pipeline and damage were monitored during the process of displacement, and the topography of the ground surface was surveyed. The pipeline damage was recorded after it was excavated at the conclusion of the test. The experimental assembly was simulated numerically to indicate the extent of the numerical model necessary to make reasonable predictions of the response of the pipeline to permanent ground displacements. This paper reports on some strain data collected during the experiment and on the numerical simulation effort.

Keywords: Lifelines, Concrete pipelines, Ground rupture, Structural health monitoring

INTRODUCTION

Concrete segmental pipelines are particularly vulnerable to damage by ground rupture, whether due to seismic causes or ground movement associated with land slides. A static ground rupture test with a buried concrete pipeline is described in this paper, as well as an effort to numerically simulate the consequences of permanent ground displacements (PGD) on pipelines. The experiment was performed in 2009 in the NEES (Network for Earthquake Engineering Simulations) Large-Scale Lifelines Testing Facility at Cornell University.

The focus of the project is on the structural health monitoring of buried lifelines and detection of damage imparted to pipelines by permanent ground movement. The experiment described is one in a series of four tests, all centered on the development of the structural health monitoring and damage detection. The experimental test bed and the test specimen (pipeline) are described first, followed by some data recorded

¹ Department of Civil and Environmental Engineering, University of Michigan, Ann Arbor, U.S.A.; e-mail corresp. author: rlmich@umich.edu.

² School of Civil Engineering, Purdue University, West Lafayette, IN, U.S.A.

³ Department of Civil and Environmental Engineering, Virginia Tech, Blacksburg, VA, U.S.A.

⁴ Department of Civil Engineering, Merrimack College, Andover, MA, U.S.A.

during the test. The modeling effort is presented to indicate that the loads induced in the pipeline and the damage incurred, can be reasonably modeled by numerical techniques.

THE TEST BASIN AND INSTRUMENTATION PLAN

Pipeline and the Test Basin

The pipeline was assembled out of five 2.44 m concrete segments, 42 cm in outer diameter, inside diameter of 30.5 cm, and was assembled in a test tank of about 13.4 m by 3.4 m. The pipes were manufactured by Hanson, Inc. (Rhode Island), according to ASTM C76 and C655 specifications (ASTM 2008a, 2008b). A dense array of sensors including potentiometers, strain gauges, electric conductivity, acoustic emission sensors, and load cells were installed along the length of the pipeline to measure the pipeline response to ground displacements. A view of the test basin with buried pipeline is illustrated in Fig. 1(a). Permanent displacement was induced by movement of one portion of the test basin, as indicated in Fig. 1(b). The angle of the simulated fault was 50° to the longitudinal pipeline axis, taken after a water main crossing the Hayward fault (near San Francisco, U.S.A.).



Figure 1. (a) Test basin, and (b) plan view of the experimental layout.

The pipes were assembled on an 0.20 m layer of medium sand, the joints were grouted, and the entire pipeline was backfilled with a 1.22 m layer of sand (more than 100 tons of poorly graded sand with $D_{50} = 0.67$ mm, uniformity coeff. $C_u = 3.83$ and curvature coeff. $C_c = 0.94$, with moisture content ranging from 3.5 to 5.3%, and dry density 1,668 to 1,703 kg/m^3). The sand was placed in 6 lifts, each compacted with 4 passes of a vibratory plate compactor to reach relative compaction (ratio of dry density to maximum dry density) of about 80%. A 10-cm grid was spray-painted on the surface of the backfill for easier observation of the surface displacements.

Instrumentation Plan

A dense array of sensors was installed throughout the buried segmented concrete pipeline in an effort to monitor deformation and failure modes during PGD. An elaborate instrumentation plan was followed to measure translational and rotational movement of the segmented pipeline joints. Four sets of four linear variable differential transducers (Novotechnik TR100 LVDT) were installed at joints #1 through #4, totaling 16 LVDTs for the complete pipeline, Fig 2(a). The LVDT wires were brought outside the basin through an opening in the basin wall near the location where the pipeline was mounted on the reaction plate. The LVDTs installed in each joint were designed to directly measure relative joint translation and rotation along the length of the pipeline.

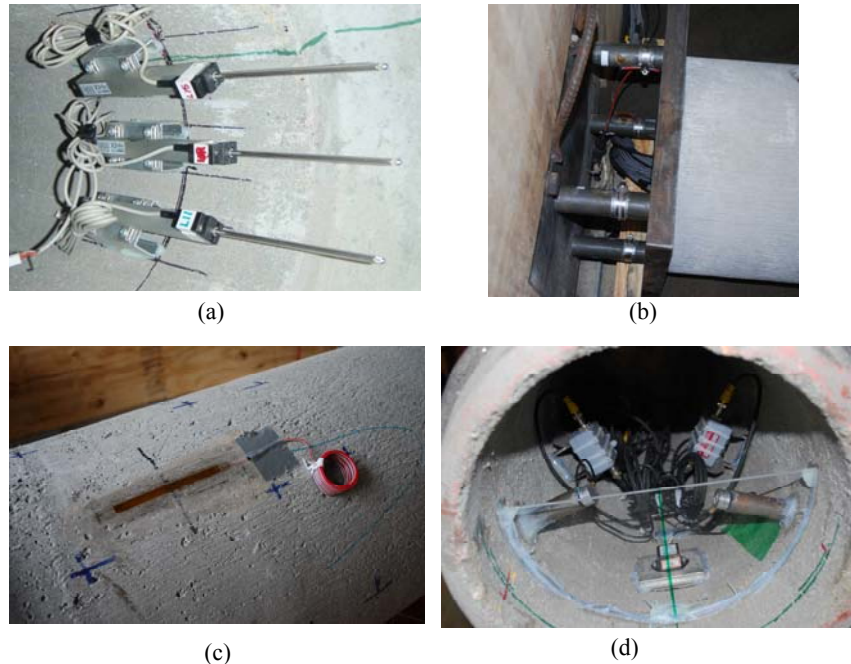


Figure 2. (a) LVDTs, (b) load cells at the pipe's end, (c) strain gauge, and (d) acoustic emission sensors.

At each of the two ends of the pipeline, four load cells were installed, Fig. 2(b), to measure the axial force induced during the test. Each load cell consisted of a steel thick-wall pipe instrumented by a rosette strain gauge array. Precise calibration tests for determining axial force from measured strain were conducted before the test.

In addition to measuring joint movement, deformation along the pipe was monitored using strain gauges, Fig. 2(c). Strain gauges (Vishay N2A-06-40CBY 350 Ω metal foil gauges) designed for measuring concrete strain on the surface of a concrete structure were mounted longitudinally along the length of the pipeline. The long gauge length (101.6 mm) allows strain integration along non-homogeneous specimens. Six strain gauges were placed equidistant along a single pipe segment, three on each side of the pipe. These six strain gauges allow for the measurement of axial strain and curvature at three sections of each pipe segment. Axial strain at a section is calculated by taking the average of the two strain measurements, and the flexural response of the pipe at a given section is calculated using the difference between the strain gauge readings on opposite sides. An additional 8 strain gauges were mounted circumferentially on the bells of pipe segments near the fault line, namely joints #2 and #3. These eight gauges were installed to measure the hoop strain at the pipeline connections. During installation of the strain gauges, the rough

concrete pipe surface was ground smooth and then a very thin and smooth surface epoxy layer was applied. The epoxy layer was delicately cleaned by fine sand paper followed by additional cleaning using acid and base solution. Strain gauges were firmly mounted above the smoothed epoxy surface using strain gauge bonding adhesive.

Additionally, tape sensors for macro-crack detection, and acoustic emission sensors, Fig. 2(d), were used, but these results are not reported here. More information regarding instrumentation can be found in Kim *et al.* (2010).

EXPERIMENT

Deformation of the pipeline and damage were monitored during the process of displacement. The total forces induced in the pipeline were monitored by the load cells at the reaction plates at both ends of pipeline. The North portion of the test basin was translated in the South-East direction, Fig. 1(b), in 12 equal increments of 2.54 cm, at the speed of 0.5 cm/s, using 4 actuators (static test simulating a ground rupture, but not earthquake shaking). The forces induced at the reaction plates were recorded. A substantial drop of the force was measured during the 12th translation increment. At that time the pipe was substantially damaged and the test was brought to an end. The pipeline damage was visually inspected after it was excavated at the conclusion of the test.

MODELING OF SOIL-STRUCTURE INTERACTION

Finite Element Model

The commercial finite element program ABAQUS/CAE (2008) version 6.8-1 was used to model the large scale test. The explicit solution procedure was chosen, as it is highly efficient for solving three-dimensional contact problems with large deformation containing discontinuities.

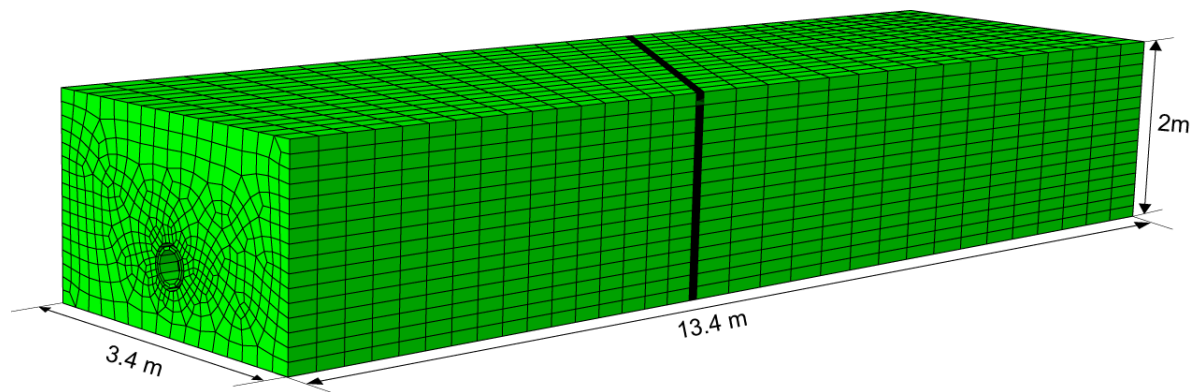


Figure 3. Simulated test basin.

The initial discretization of the test basin is depicted in Fig. 3 and models of the pipe segments are illustrated in Fig. 4. Both the soil and the pipes were modeled using 8 node linear brick elements with reduced integration and hour glass control. A coarse mesh with 22,602 nodes (18,952 elements) was chosen for initial analysis; a more refined mesh was used in regions close to the pipe and the fault. A more refined model with 350,000 nodes was also used, but the processed data was not yet available at the time of writing this report. Elastic-perfectly plastic model was used for the soil, and the concrete pipes were

modeled as elastic with damage induced beyond certain strain threshold. The joints between the pipes have a snug fit, and the grout was not modeled.

Even though calculations were carried out on five processors, the time for simulations was excessive; therefore, in these preliminary computations the bell of the pipe segments (Fig. 4(a)) was replaced by a simpler slide-in connection (Fig. 4(b)).

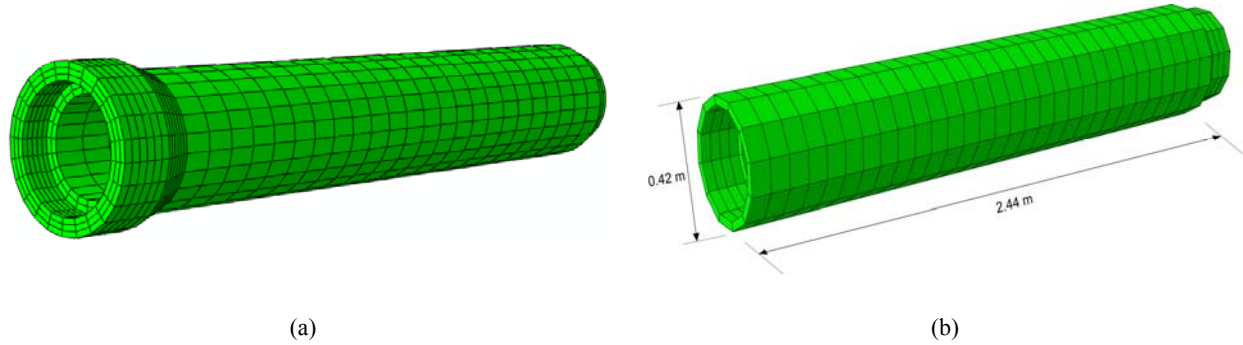


Figure 4. (a) Model of the pipe segment, and (b) simplified model for preliminary calculations.

The soil-pipe contact was modeled as a master-slave contact (the pipe being the master; the nodes of the master surface can penetrate the slave surface but not vice versa). A refined mesh was used on the slave surface to minimize excessive penetration. The contact is unilateral, and no tensile stresses across the boundary were permitted. Isotropic surface friction was assumed, with coefficient of friction $\mu = 0.3$, typical of clean sand–formed concrete interface (NAVFAC 1986). The bell-spigot contact between two pipes was modeled in a similar manner (the spigot being the master surface).

To allow for large displacements in the mesh near the fault, Arbitrary Lagrangian-Eulerian (ALE) adaptive meshing scheme was used. To prevent mesh distortions, element shapes were independently optimized.

Soil and Concrete

The soil was modeled as elastic-perfectly plastic. Isotropic elasticity was assumed with the Young's modulus $E = 30$ MPa and Poisson's ratio $\nu = 0.25$. The Drucker-Prager (1952) function (with no cohesive component) was used to model the soil yielding

$$F = t - p \tan \beta = 0 \quad (1)$$

and the non-associative flow rule was adopted with the plastic potential in the form

$$G = t - p \tan \psi^* = C \quad (2)$$

where

$$t = \frac{1}{2}q \left[1 + \frac{1}{K} - \left(1 - \frac{1}{K} \right) \left(\frac{r}{q} \right)^2 \right]; \quad p = -\frac{1}{3}\sigma_{kk}, \quad q = \sqrt{\frac{3}{2}s_{ij}s_{ij}}, \quad r = \sqrt{\frac{9}{2}s_{ij}s_{jk}s_{ki}} \quad (3)$$

and s_{ij} is the deviatoric stress tensor. The material properties β and ψ^* in eqs. (1) and (2) are related to internal friction angle ϕ and dilatancy ψ angle as

$$\tan \beta = \frac{6 \sin \phi}{3 - \sin \phi}, \quad K = \frac{3 - \sin \phi}{3 + \sin \phi}, \quad \tan \psi^* = \frac{6 \sin \psi}{3 - \sin \psi}$$

For the sand used in the experiment, the internal friction and the dilatancy angles were taken equal to 40° and 5° , respectively. This translates in the following Drucker-Prager parameters: $\beta = 58.6^\circ$, $\psi^* = 10.2^\circ$, and $K = 0.778$. The value of 5° for the dilatancy angle was selected, based on Bolton (1986), and it is likely to be a low estimate when related to the relative compaction of 80%.

The concrete pipes were modeled as elastic with damage induced beyond certain strain threshold. The damage was described with the Concrete Damage Plasticity (CDP) model, based on the developments of Lubliner *et al.* (1989) and Lee and Fenves (1998). Isotropic Hooke's law was adopted in the elastic range, with elastic parameters for undamaged concrete $E_0 = 20$ GPa and $\nu = 0.19$.

Concrete is subjected to *plastic damage* in both the tensile and the compressive regime. This damage is manifested in softening behavior and in degradation of elastic properties. In uniaxial tension, stress-strain response follows a linear elastic relationship until failure stress σ_{t0} ; this marks the onset of micro-cracking, and further process is characterized by softening and elastic degradation, as indicated in Fig. 5(a). Because the reinforcement is not modeled, the softening behavior is not taken as a sudden loss of material integrity, as is often assumed for pure concrete.

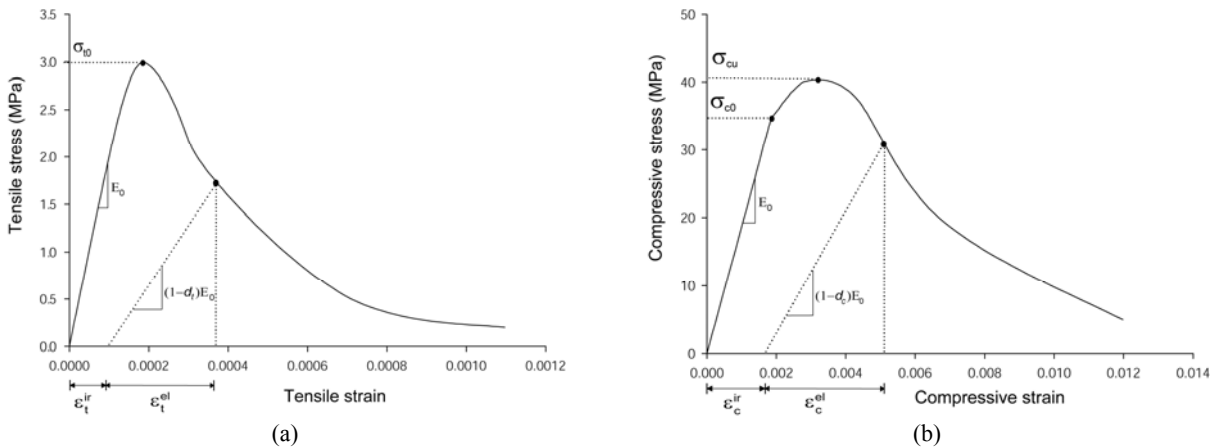


Figure 5. (a) Behavior of (lightly reinforced) concrete in tension, and (b) compression.

The behavior in compressive regime is marked by much larger stress magnitude upon reaching the onset of micro-cracking at stress σ_{c0} , Fig. 5(b), and a significant range of hardening before reaching the ultimate stress σ_{cu} . The softening behavior is then “gentler” (notice the difference in both the stress and strain scale in Figs. 5(a) and 5(b)). The degradation behavior is characterized by two independent damage variables: d_t and d_c , with the value of zero for undegraded (undamaged) concrete, and unity for fully damaged material

($0 \leq d \leq 1$). Both hardening (in compression) and softening behavior is governed by non-associative flow law. The details are omitted here, and the Reader is directed to the papers by Lubliner *et al.* (1989) and Lee and Fenves (1998).

EXPERIMENTAL AND MODEL RESPONSE TO GROUND RUPTURE

Axial Force Induced During the Test

The load from the pipeline was transferred through the reaction plates (Fig. 2(b)) to the test basin frame, and the force was monitored with four load cells at each end of the pipeline. The forces recorded at both the North (red) and the South (black) and are illustrated in Fig. 6. Each displacement increment took 5 seconds; the intervals between the displacement increments were longer, but for the purpose of presentation they are reduced in Fig. 6 to about 5 seconds. Some relaxation of the force was detected when the test basin was kept stationary between the displacement increments. The forces induced at the reaction plates were increasing with every stroke, with the exception of increments #5 and #7, when some drop in the force was detected. The maximum force at both ends reached about 37 tons during the 12th displacement increment, and it dropped down rapidly to about 24 tons at the end of that increment. At that time the pipe was substantially damaged and the test was brought to an end.

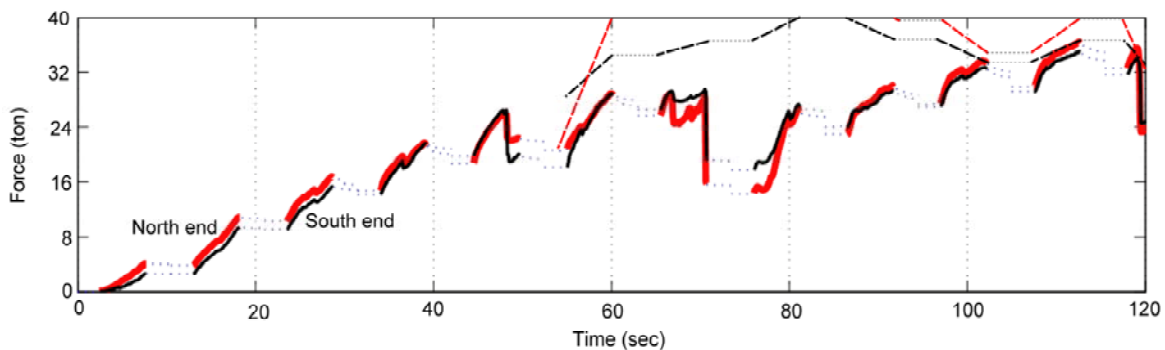


Figure 6. Compressive reactions at the ends of the test basin.

In the preliminary calculations a simplified model of the bell-and-spigot joints was used. The joints were modeled with a snug fit (no gap) and no grout. Consequently, the initial stiffness of the model pipeline exceeded that of the physical pipe assembly, and the calculated axial forces during the first few displacement increments exceeded significantly the measured magnitudes. However, after some damage at the joints has occurred, the calculated forces dropped down (after 5 displacement increments) to a level measured in the experiment. These forces, past the fifth displacement increment, are indicated with dashed lines in Fig. 6 (black for the South end).

While the magnitude of FEM-simulated forces in the pipeline coincides with those measured in the final stages of the experiment, it is clear that the model of the joints needs to be improved in order to more accurately predict the forces at the early stages of the loading. The next-generation model will include grouted joints, with the mortar described with the plastic damage model, and with the initial stiffness considerably lower than that for the concrete.

Strains in the Pipe Segments

Concrete strains were monitored on pipes #2, 3, and 4, with strain gauges installed at three locations along each pipe on two opposite sides, as illustrated in Fig. 7(a). The average strain measured on pipe #2 at

location SG1 and SG1' is illustrated in Fig. 7(b) as function of the actuation step in the process of test tank displacement. The strain difference, indicative of curvature of the pipe, is given in Fig. 7(c). The respective values calculated from the finite element model are presented in Fig. 7(d) and (e).

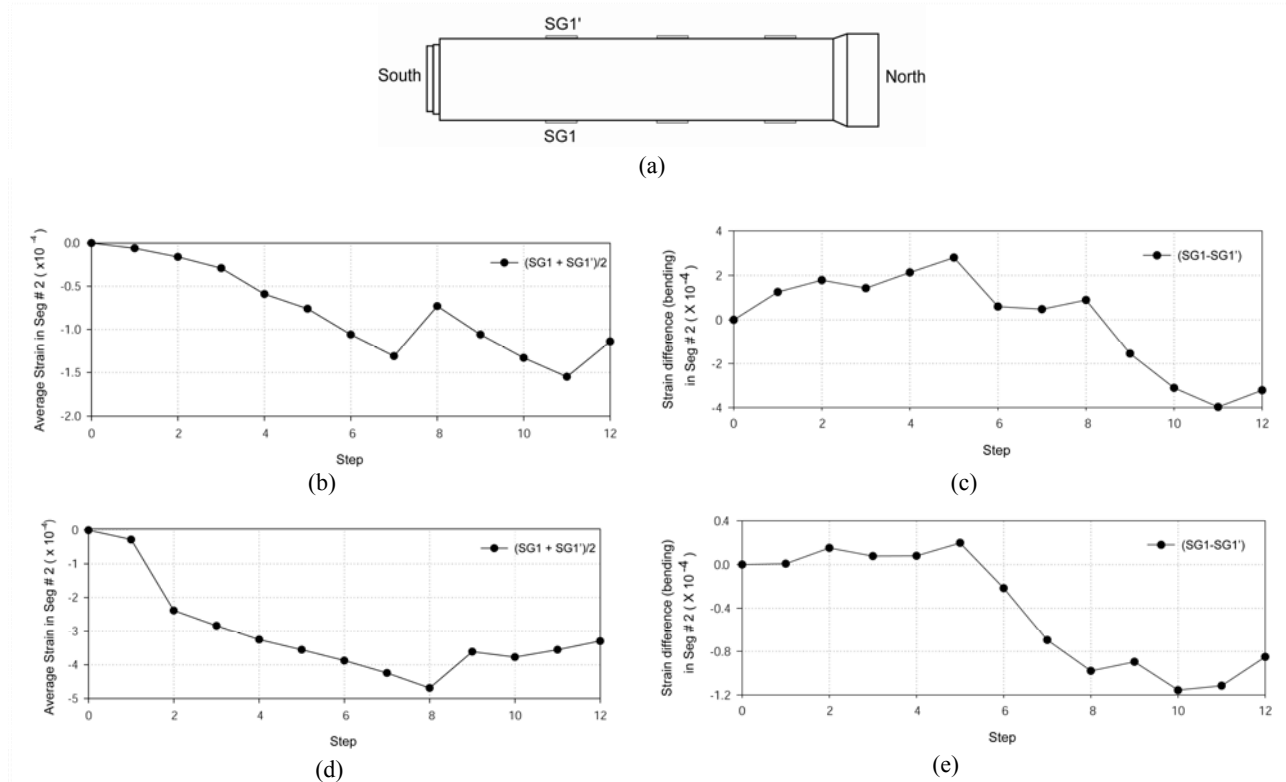


Figure 7. (a) Location of strain gauges on segment #2, (b) measured average strain (compression negative), (c) measured strain difference, (d) calculated average strain, (e) calculated strain difference.

The discrepancy in the strain measured and calculated is more than threefold in the early stages of the test. The reason in this discrepancy was identified in the crude model of the joints that renders the system stiffer than the physical pipeline, resulting in axial forces exceeding significantly the true values. The second possible reason for this discrepancy is in the choice of pipe concrete elastic properties. The consequences of the model inaccuracies are also seen in smaller calculated strain difference (Fig. 7(c) and (e)), indicative of pipe curvature. However, the evolution of calculated and measured strains is qualitatively similar. Both the joint model and the concrete properties will be refined in the ongoing modeling effort.

Joint Rotation and Pipeline Damage

The ground rupture after the last displacement increment is shown in Fig. 8(a). As expected, the rupture is characterized by an anti-symmetric pattern. Excavated pipeline is shown in Fig. 8(c), with severe damage in joints #2 and #3 (see also Fig. 8(b)). This damage is also indicated in numerical calculations, with the tensile damage variable d_t illustrated in Fig. 8(d).

Relative rotation in joint #2 was measured to be 5.9° and the one calculated from the finite element model reached 5.65° . The respective numbers for joint #3 are: 6.5° (measured) and 5.45° .

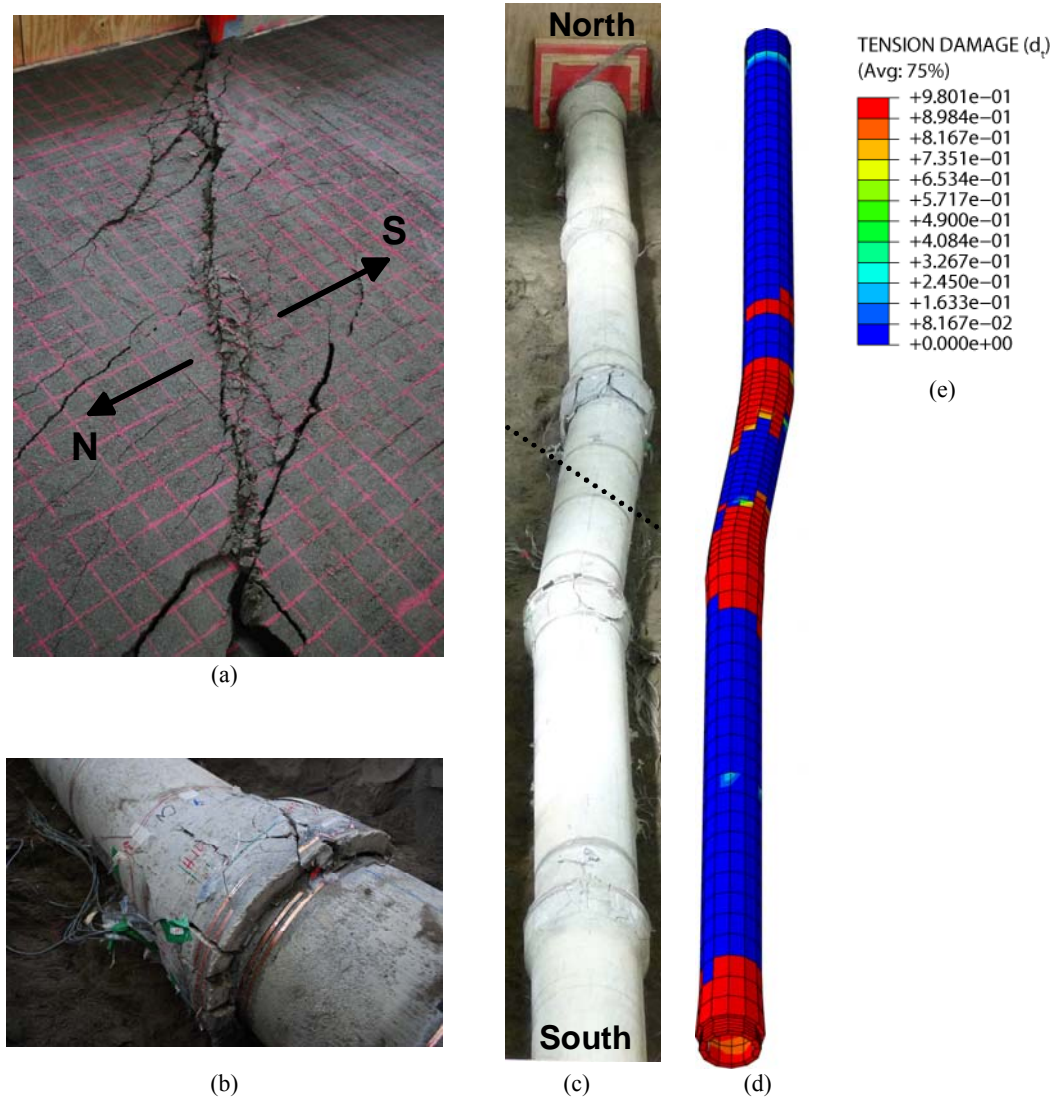


Figure 8. (a) Ground rupture, (b) damaged joint, (c) excavated pipeline after the test, (d) numerically simulated damage, and (e) color scale for the tensile damage variable d_t .

CONCLUDING REMARKS

A primary objective of this study was to observe the sequential failure of concrete segmented pipelines subjected to permanent ground displacements. A real-time monitoring system was utilized to observe the displacement of the pipe segments during the execution of ground faulting. Two evident failure modes of the pipeline joints were found by post-event visual inspection: combined rotation and contraction failure as well as compressive telescoping failure (penetration of the spigot into the bell section of the adjacent pipe). Based on the analysis of the sensor data, a gradual failure sequence of the buried concrete segmented pipeline was also identified. Specifically, as the ground gradually moved, grout crushing occurred in the pipeline joints thereby allowing each concrete pipe segment to come into direct contact with the adjacent pipe. Grout crushing began at the joints adjacent to the fault line and propagated out toward the end joints consecutively. With the increase in the fault displacement, the concrete in the joints

of the pipeline underwent progressive damage, with the most severe damage in the joints closest to the fault line.

The analysis of the test included the finite element model of the entire test basin and the pipeline. This preliminary effort was focused on qualitatively mimicking the deformation and damage processes, and identifying elements of the model that need modification. The component of the model that requires a major refinement is the bell-and-spigot joint. It was concluded that appropriate modeling of the joint stiffness (including grout) is crucial to the simulation of quantitatively proper response of the pipeline to ground rupture.

ACKNOWLEDGEMENTS

The work presented in this paper was supported by the National Science Foundation through grant CMMI-0724022. This support is greatly appreciated. We also thank the Cornell University team of the NEES Large-Scale Lifelines Testing Facility for their help in performing the experiment.

REFERENCES

- ABAQUS /CAE (2008). User's Manual (v. 6.8-1). Dassault Systèmes Corp., Providence, RI, USA.
- ASTM (2008a). Standard Specification for Reinforced Concrete Culvert, Storm Drain, and Sewer Pipe. ASTM International.
- ASTM (2008b). Standard Specification for Reinforced Concrete Culvert, Storm Drain, and Sewer Pipe. Designation: C 76-08a, ASTM International.
- Bolton, M.D. (1986). "The strength and dilatancy of sand." *Géotechnique*, Vol. 36, No. 1, 65-78.
- Drucker, D.C. and Prager, W. (1952). "Soil mechanics and plastic analysis or limit design." *Quart. Appl. Math.*, Vol. 10, No. 2, 157-165.
- Kim, J., O'Connor, S., Nadukuru, S., Pour-Ghaz, M., Lynch, J.P., Michalowski, R.L., Green, R.A., Bradshaw, A. & Weiss, W.J. (2010). "Behavior of full-scale concrete segmented pipelines under permanent ground displacements." *Proceedings of SPIE Conference: Smart Structures/NDE 2010*, San Diego, CA, March 7-11, 2010.
- Lee, J. and Fenves, G.L. (1998). "Plastic-damage model for cyclic loading of concrete structures." *ASCE J. Eng. Mechanics*, Vol. 124, No. 8, 892-900.
- Lubliner, J., Oliver, J., Oller, S. and Onate, E. (1989). "A plastic-damage model for concrete." *Int. J. Solids Struct.*, Vol. 25, No. 3, 299-326.
- NAVFAC (1986). Design Manual DM 7-02: Foundations and Earth Structures. September 1986.